City Research Online

City, University of London Institutional Repository

Citation: Kong, D. & Fonseca, J. (2019). On the kinematics of shelly carbonate sand using X-ray micro tomography. Engineering Geology, 261, 105268. doi: 10.1016/j.enggeo.2019.105268

This is the accepted version of the paper.

This version of the publication may differ from the final published version.

Permanent repository link: https://openaccess.city.ac.uk/id/eprint/22702/

Link to published version: https://doi.org/10.1016/j.enggeo.2019.105268

Copyright: City Research Online aims to make research outputs of City, University of London available to a wider audience. Copyright and Moral Rights remain with the author(s) and/or copyright holders. URLs from City Research Online may be freely distributed and linked to.

Reuse: Copies of full items can be used for personal research or study, educational, or not-for-profit purposes without prior permission or charge. Provided that the authors, title and full bibliographic details are credited, a hyperlink and/or URL is given for the original metadata page and the content is not changed in any way.

City Research Online: http://openaccess.city.ac.uk/ publications@city.ac.uk

On the kinematics of shelly carbonate sand using X-ray micro tomography

Deqiong Kong [1], Joana Fonseca [2*]

*Corresponding Author

Joana.Fonseca.1@city.ac.uk

ABSTRACT

Shelly carbonate sands are highly compressible soils due to the susceptibility of their loose and intricate fabric to collapse under loading. An accurate assessment of the physical phenomena taking place at the grain-scale is critical for a better understanding and modelling the mechanical behaviour of this material. This paper presents a study on the grain kinematics of shelly carbonate sand through analysis of in-situ 4D X-ray tomography images acquired during oedometer compression. Two sands from the Persian Gulf, with coarse and fine grading, were investigated. An adaptive watershed segmentation technique is used here to identify the grains in the image(s) prior to loading and a digital volume correlation (DVC) technique is employed to obtain the displacement field of each grain under loading. The displacement fields are used to reconstruct the grains in their new positions and compute the associated translation and rotation. An extensive statistical analysis was carried out to demonstrate the effect of grain morphology and local fabric (coordination number) on grain kinematics. The new findings presented here shed light on the mechanisms of grain rearrangement leading to the compressible fabric of shelly carbonate sands and, are also critical, to better understand other weak grained sands and/or silica sands with an open fabric.

KEYWORDS: Calcareous soils; Fabric/structure of soils; Offshore engineering; Particle-scale behaviour; Grain kinematics; Compressibility

---

1 College of Civil Engineering and Architecture, Zhejiang University, Hangzhou, China, ORCID: 0000-0002-9122-9294

2. Department of Civil Engineering, City, University of London, UK, ORCID: 0000-0002-7654-6005

1. Introduction

Shelly carbonate sands are of biogenic origin and comprise grains of low hardness and angular shapes forming an interlocked open fabric (e.g. Semple, 1988; Golightly, 1989; Coop, 1990; Wang et al., 2011; Fonseca et al., 2015). The high compressibility has been identified as one of the most important factors affecting their mechanical behaviour (e.g. Yasufuku et al., 1995; Randolph et al., 2004; Dijkstra et al., 2013; Shahnazari et al., 2013). When subjected to loading, the change in soil fabric is achieved through grain rearrangement by means of slippage and rotation. However, for shelly sands with interlocked internal structure and structurally weak grains, this process could also require prior grain damage such as chipping of asperities as a means of 'unlocking mechanism' (Mesri and Vardhanabhuti, 2008). These unlocking mechanisms associated with the large voids, are believed to lead to a temporary loss of contacts and consequently to an abrupt fabric collapse. A more scientific understanding of these grain-scale phenomena is critical for an accurate modelling of shelly soils and, indeed, other weak grained sands or silica sands with an open fabric (Bolton, 2000).

The compressibility of granular soils can be modelled using two methods: discrete element modelling and analytical approaches. A desirable characteristic for both methods is that they make use of parameters with a physical meaning derived from the microstructure of the soil and their evolution under loading. Meidani et al. (2017) proposed an analytical compression model based on the contribution of micro-scale mechanics to the change of active and inactive voids. Discrete element modelling techniques enable the simulation of granular interactions, however, the challenges in defining soil fabric and realistic particle shapes limit their application to shelly carbonate sands. Recent work by the authors (Nadimi and Fonseca, 2018) used the true representation of the soil fabric and grain shapes obtained from three-dimensional (3D) images, to model the individual grains and their interactions in a framework of combined discrete-finite-element method. In this model, the shelly grains are allowed to interact and deform according to an appropriate constitutive model, as well as, frictional contact conditions and the contact response results from the deformation of contacting bodies. The development and validation of this approach requires the kinematical behaviour of the soil grains obtained from experiments.

Imaging techniques such as X−ray computed tomography (μCT) has been pivotal to contribute insights into the deformation of the internal structure of soil under loading (e.g. Matsushima et al., 2010; Fonseca et al 2013a; Cil and Alshibli, 2014; Mahbub and Haque, 2016). A key step in analysing μCT images of granular materials at a scale where grains can be identified is to separate the individual grains using segmentation techniques based on watershed algorithms (Beucher and Lantuejoul, 1979; Meyer 1994). The main challenge of watershed segmentation is the treatment of ill-segmentation, i.e. when an individual grain is mistakenly segmented into several sub-grains, or, several grains are combined as one. Ill-segmentation potentially affects all types of sand and has been effectively alleviated in recently proposed watershed algorithms (e.g. Wählby et al., 2004; Fonseca, 2011; Shi and Yan, 2015). This problem, however, can be more severe for shelly carbonate grains due to the presence of highly irregular grain shapes and intra-granular voids, as discussed by Kong and Fonseca (2018).

Once the individual grains are identified in the initial stage, a statistical analysis of various grain indices, such as, size, shape and orientation can be carried out for the whole sample (e.g. Fonseca et al., 2013a, 2013b) to characterise the material. To investigate grain kinematics, in terms of rotation and translation of the grain, it is required to obtain the position of the grain in the subsequent loading stages, in other words, in its deformed position. Existent techniques, previously developed for silica sands, include the ID tracking method (e.g., Smit, 2010; Andò et al., 2012) that consists of attributing an identity to each grain, using an analogy to an ID card that in this case contains the characteristics of the grain that make it unique in relation to other grains in the sample (e.g., shape, size, etc.). The effectiveness of this method is, however, largely susceptible to watershed segmentation discrepancies and the occurrence of grain damage. Most importantly, since the essence of the ID-tracking method is to identify a given grain in the target (deformed) image that has properties close to the grain in the reference (undeformed) image, the occurrence of ill-matching (*i.e.* when a grain cannot be tracked due to small changes in its outline and it is instead wrongly matched with a different grain) will result in an erroneous measurement of grain displacement.

In this paper, an alternative to the ID tracking method is used, in which, the displaced position of a grain is “reconstructed” based on its prior-to-loading position and the displacements of each voxel (3D pixel) forming the grain. The displacements are obtained by correlating the intensity patterns of the reference and the target images, using the digital volume correlation (DVC) technique originally proposed by Bay *et al.* (1999). This is a powerful tool as evidenced by its increasing use for biomechanics, material science and experimental mechanics studies (e.g. Liu and Morgan, 2007; Bay, 2008; Hall et al., 2010; Leclerc et al., 2011; Hussein et al., 2012). This DVC-based new method is particularly suitable for shelly carbonate grains that are susceptible to surface damage by chipping of asperities and ill-segmentation that potentially make grain tracking impractical.

This paper first describes the experiments, including the set-up of the one-dimensional compression tests and the acquisition of the X-ray micro tomography images. The image analysis part investigates the evolution of the grain morphology and coordination number. Following that, the DVC-based technique is used to quantify grain rotation and translation. Finally, a discussion on the effect of grain morphology and fabric on grain kinematics under one-dimensional compression is presented.

2. One-dimensional tests and image acquisition

Two uncemented carbonate sands from the Persian Gulf, a coarse and a fine sand, denoted CS and FS respectively hereafter, were investigated. The median grain sizes of CS and FS are approximately 1.9 mm and 0.4 mm, respectively. *In-situ* one-dimensional compression tests were carried out using a mini-oedometer placed inside a Nikon XTH 225 ST scanner (Fig. 1), at the Research Complex at Harwell (UK). Three-dimensional (3D) X-ray tomography images were acquired with a spatial resolution of 9.57 μm at various stages throughout loading, as shown in Table 1. The accelerating voltage of the scanner was set to be 90 kV for the CS and 110 kV for the FS. For the construction of each 3D image, a total of 3142 projections were collected with an exposure of 500 ms per projection. During an X-ray scanning, the objects with various material compositions and densities within the sample attenuate different levels of X-ray beam energy, represented by distinct intensity values of the voxels. The contrast of differing intensity levels allows for differentiation of the features within the image. The sample container was made of Perspex with a diameter of 14 mm and a thickness of 2 mm, and the transverse deflection of the container was limited to 0.003 mm under the ultimate loading. Friction between the container and the x-ray window was avoided by allowing a 1 mm gap. The vertical load was exerted by a micrometre and monitored by a load cell with a capacity of 500 N. The sizes, in voxel, of the scanned images after cropping were 1536 × 1536 × 1600 and 1536 × 1536 × 1536 for CS and FS, respectively. Top view slices through the 3D images of both samples are shown in Fig. 2a and 2b.

3. Image analysis at the grain scale

3.1. Image segmentation and grain morphology

The segmentation technique employed to identify the individual grains in the scanned images is briefly explained here. Each image was binarised using the double intensity threshold method (Henry et al., 2013) first, and then segmented using an adaptive segmentation technique proposed by Kong and Fonseca (2018). Top view slices through the segmented images of CS and FS are presented in Fig. 2c and 2d. Prior to compression, approximately 700 grains were identified in CS and over 150,000 in FS.

The quantification of grain morphology in terms of size and shape was done following the procedure discussed in Kong and Fonseca (2018). The size of a grain is described by the length of the three orthogonal axes termed the major (*a*), intermediate (*b*) and minor (*c*) axes, obtained from principal component analysis (Fonseca 2011). The shape indices include elongation (I_E), flatness (I_F), convexity (I_C) and sphericity (I_S), formulae provided in Appendix. They all take dimensional values between zero and one, with the latter corresponding to the most extreme cases. The median values for these parameters are presented in Table 2.

Fig. 3 shows the evolution of grain sizes (given by *a*, which better reproduce the sieve results) throughout the loading. It can be inferred from Fig. 5a that the number of grains with sizes between 0-1000 μm increases slightly, while that between 1800-4500 μm decreases slightly, under loading. This suggests a small reduction in grain size as a result of chipping of asperities and sharp corners; since grain splitting was not observed for the stress level investigated here (the fluctuations are likely to be related to the small number of grains in the sample. Interestingly, the fine soil shows marginal grain damage (Fig. 5b), which can be because due to the wider range of grain sizes as discussed in the work by Altuhafi & Coop (2011). The statistical analysis of the shape parameters through the loading stages did not show any conclusive observation.

3.2. Contact detection and coordination number

Following the application of the watershed algorithm, the 'watershed ridges' between the grains in contact were removed from the solid phase. For the detection of grain contacts, it is necessary to temporarily expand the grain in analysis so that the contact between it and the neighbouring grains can be established. For clarity, this is illustrated by a 2D example image shown in Fig. 4a, where the grain of interest, labelled n_0, is potentially in contact with the surrounding grains labelled n_1, n_2 ..., n_6. The surrounding grains are isolated first (Fig. 4b), and the grain of interest is expanded (Matlab function: *imdilate*) and given a temporary label N (Fig. 4c), which is greatly larger than the total number of grains in the image to avoid possible mistakes. The isolated grains are then superimposed and there will be overlapping areas where label values are larger than N can be identified (Fig. 4d), based on which the labels of grains in contact with grain n_0 are identified and its coordination number can be calculated accordingly. To avoid two 'not-in-contact' grains being mistakenly identified as a contact pair, only the grains strictly attached to the same watershed ridges are searched using the algorithm described here, which also greatly improves the searching efficiency. This contact detecting algorithm proves to be computationally efficient and the corresponding calculation for the FS containing more than 150,000 grains can be completed within in 10 minutes. This constitutes a significant improvement in computational efficiency when compared with the algorithm used in Fonseca (2011) and Fonseca et al. (2013b).

The coordination number (CN) is investigated here as a measure of the packing density, based on the average number of contacts per particle (Fonseca et al., 2013b) The median values of CN measured in the image at each stage throughout loading are presented in Table 2, for CS and FS. The calculated distributions of CN throughout loading are shown in Fig. 5. For CS (Fig. 5a), the number of the grains with smaller CN values appears to increase despite the fact that the sample becomes more compacted. This observation can possibly be related to chipping of sharp corners that result in the loss of contacts. The fluctuations caused by the limited number of grains in the CS, however, prevent a very conclusive remark. For FS (Fig. 5b), the number of grains with high CN values between 8 and 16 increases, while that between 1 and 6 decreases significantly, in agreement with the formation of a more compacted packing. For silica sands, an increase in the average CN value under loading was also observed (Fonseca et al. 2013b).

4. Grain kinematics

4.1. Parameters definition

The translation of a grain was calculated as the change in the position of its centroid, expressed as:

$$\Delta = [\mathrm{mean}(x_{\mathrm{t}}), \mathrm{mean}(y_{\mathrm{t}}), \mathrm{mean}(z_{\mathrm{t}})] - [\mathrm{mean}(x_{\mathrm{r}}), \mathrm{mean}(y_{\mathrm{r}}), \mathrm{mean}(z_{\mathrm{r}})] \quad (1)$$

For the quantification of rotation, a new scalar rotation factor is proposed here, defined as follows:

$$\delta = \left\|\beta_{1,t} - \beta_{1,r}\right\| + \left\|\beta_{2,t} - \beta_{2,r}\right\| + \left\|\beta_{3,t} - \beta_{3,r}\right\| \quad (2)$$

where β_1, β_2 and β_3 are the three orthogonal principal components (directions) of the major, intermediate and minor principal axes of the grain obtained using the principal component analysis (Matlab function: *pca*). For a grain having two (or all) principal axis with similar lengths, it is possible that the order of the three axes is not the same at the target and reference positions, and in some cases, the direction of some axes could even be ‘reversed’. Therefore, for an arbitrary principal component $\beta_{i,r}$, its counterpart ($\beta_{i,t}$) is chosen when $\left|\beta_{i,r} \cdot \beta_j\right|$ has the largest value for j = 1, 2 and 3 (with the smallest intersection angle). Then, $\beta_{i,t}$ is determined as:

$$\beta_{i,t} = \mathrm{sign}(\beta_{i,r} \cdot \beta_j) \cdot \beta_j \quad (3)$$

where the first term is used to consider the possibility of a ‘reversed’ direction.

4.2. DVC-based reconstruction of grains

For a reference grain (G_r) in the reference image (IM_r), the corresponding displacements extracted from the displacement field throughout the image, calculated from DVC, are used to reconstruct the target grain (G_t) in the target image (IM_t). An open source DVC code provided by Bar-Kochba *et al*. (2015) was used and further details can be found in the original paper. The code utilises a fast Fourier transform based cross-correlation formulation in conjunction with the iterative image deformation method (Huang et al., 1993; Jambunathan et al., 1995) and proves to be efficient in analysing general non-linear 3D deformations. The size of each grid element in the DVC mesh was defined as 8 × 8 × 8 (in voxel), and the DVC outputs are three displacement matrices (in *x*, *y* and *z* directions). These matrices were then expanded through linear interpolation to generate matrices with the same size as the segmented images.

The coordinates of an arbitrary grain, formed by a total number N of voxels, in the segmented image are represented as $[x, y, z]$, where x, y and z are $N \times 1$ vectors. Then the displacements, denoted as $[u_x, u_y, u_z]$, of this grain can be extracted from the expanded displacement matrices (MATLAB function: *find*, *ind2sub*), and the coordinates of the grain are updated as:

$$[x_{\mathrm{t}}, y_{\mathrm{t}}, z_{\mathrm{t}}] = [x_{\mathrm{r}}, y_{\mathrm{r}}, z_{\mathrm{r}}] + [u_x, u_y, u_z] \tag{4}$$

where the subscripts r and t correspond to the quantities assessed at the reference and target positions, respectively. Figs. 6a and 6b shows an example of a binarised grain in its initial (undeformed position) and in its deformed position, respectively; together with the associated displacement field (Fig. 6c).

4.3. ID tracking method

The size and shape properties of the grains in the sample provide the basis for the ID-tracking method. For an arbitrary reference grain G_r, a searching process is performed by matching its properties with those of the grains segmented in IM_t, to find its counterpart. The properties used for the matching in the present study are: volume, principal axes length, elongation, flatness, convexity and sphericity. If the differences calculated for these properties are within a specified tolerance, taken as 20% in this study, the corresponding grain is recognised as a potential ‘target grain’. In the case of more than one such grains being found, the best match is chosen as G_t. Similar technique was used by Smit (2010) and Andò et al. (2012), where the properties considered for the tracking were the volume and surface area of the grains. The limitation of this method lies in the fact while G_r is readily derived from IM_r, its counterpart (G_t) cannot be necessarily found in IM_t, due to ill-segmentation caused by possible surface damage. For all 700 grains in CS sample only 239 could be tracked between loading stages 0-1 and 199 between loading stages 1-2, and as deformation progresses fewer grains can be tracked.

4.4. Measurements and analysis

Geometrical characteristics such as grain volume and grain shape are affected by chipping of sharp corners of shelly carbonate grains even under relative low loading as it is the case of the tests here presented. Grain damage can thus make tracking not practical. Those grains that can be, however, effectively tracked, are used here to validate the DVC-reconstruction method. The key advantage of the DVC-reconstruction method is that it is less vulnerable to grain damage since only the segmentation the grains prior to loading is required, unlike the ID-tracking method that highly relies on the accurate segmentation of the grains throughout the loading.

For a more detailed inspection, the magnitude of the translation vectors for the grains that can be tracked, *i.e.* 239 between loading stages 1-2 and 199 for loading stages 2-3, are compared in Figs. 7a and 7b. Good agreement can be observed since approximately 92% of points are located near the agreement line with discrepancies within ±10% at both loading intervals. For the rotation values the agreement was of approximately 80% with the ID-tracking method yielding slightly higher results. This is likely to be associated with ill-segmentation that alters the shape of the grain and the orientation of the principal axes, thus leading to larger rotation values. Overall, and for the large majority of the grains the agreement is good, which shows the capability of the proposed method to assess grain kinematics.

Possible sources of error associated with the DVC-reconstruction method are likely to be related to partial volume effects. While this can be alleviated by high resolution, which indeed is the case of the present study, it cannot be perfectly avoided when dealing with angular and highly irregular surfaces found in shelly grains. Important to highlight here is the advantage of the DVC-reconstruction method in providing the displaced positions for almost all grains, provided that grain detachment following grain cracking does not take place.

5. Discussion

5.1. Evolution of grain kinematics under loading

The translation mechanisms are investigated here using the distribution of the magnitude of translation vectors. For CS (Fig. 8a), relatively high frequencies can be seen for translation values above 200 μm during interval 0-1, while the higher frequencies are located between 50 and 200 μm for the two subsequent intervals. This observation suggests that intense grain movement took place initially as the grains rearrange to accommodate the imposed load for the sample with large initial voids. This initial rearrangement is not so pronounced in FS (Fig. 8b) and for both intervals the most frequent translation peak locates between 50 μm and 100 μm. Regarding the distribution of the rotation factors, also a markedly difference between the first loading interval and the two subsequent ones can be found for CS (Fig. 8c) but not for the FS case (Fig. 8d).

In order to better understand the spatial distribution of the kinematics within the sample, the grains in the CS sample have been coloured according to their rotation value, as shown in Fig. 9. It can be seen that, for the first loading interval, the grains with larger rotations are randomly distributed, which reflects the initial adjustments in the sample. For the subsequent intervals the higher rotations are located at the top half of the sample and this can be due to the use of a fixed ring oedometer and also the related to sample preparation.

The correlation between the rotation values and the magnitude of the translation vectors for each grain was investigated but no clear trend was observed. Regarding the effect of CN on grain rotation, it was observed that the largest rotation factor a grain can achieve is hindered by large coordination number values. This is expected as a grain with high coordination number (*i.e.* more contacts with neighbouring grains) is more likely to have less degrees of freedom and rotation is less likely to take place. This observation is in agreement with previous results that link the occurrence of chipping of asperities to high CN (Karatza et al., 2019) and, thus, demonstrates the need for grain damage as an unlocking mechanism to enable grain rearrangement. On the other hand, grain translation is less affected by the coordination number of the grain, as a cluster of grains, regardless of their coordination numbers, could translate as an ensemble in the direction of the loading.

5.2. Effect of grain morphology on grain kinematics

The effect of grain size and shape on the rotation and translation is examined in this section. The plot of grain rotation against grain size (given by a), shown in Fig. 10a, suggests that higher rotation values are attained by smaller grains and that larger grains are generally limited to the lowest measured rotation factors. This trend can be observed for both CS and FS (although only CS is shown).

Since the axis length do not provide any information on whether the grain is large and bulky or just has one large principal axis length, the correlation of rotation with elongation and flatness was analysed. As shown in Figs. 10b and 10c, despite the scatter, it can be seen that more elongated grains (higher I_E) and plate-like grains (higher I_F) are associated with smaller rotation values, suggesting that the grains with more elongated and plate-like shapes tend to form interlocked structures that hinder rotation. The link between grain interlocking and grain shape is also demonstrated by considering grain convexity. As shown in Fig. 10d, for grains with low I_C, i.e. with concave features, the rotation values are seen to be lower when compared with more convex grains. This is expected as the small re-entrances in the grain surface will promote interlocking. The angular features of the grain surface, captured by the high angularity values, have a similar effect, though not presented here. No expressive trend was found for the effect of I_S on grain rotation.

6. Conclusions

This paper uses a DVC-reconstruction method to quantify grain kinematics in shelly carbonate sands for sands. This technique has the advantage of overcoming limitation related to the complex morphologies and/or proneness to grain damage, for which, for which ID-tracking methods can be of limited application. Since the grain in the deformed image is identified based on the associated displacement field, this method is less affected by ill- segmentation or subtly changes in the outline of the grain. This enabled to measure rotation and translation for shelly carbonate sands under oedometer compression for the first time in the literature.

For the stress/strain level considered in this study, there is very limited grain splitting taking place for both the coarse and fine samples. However, chipping of asperities was found for the coarse sand, as indicated by the reduction in grain size and coordination number as loading progresses. This phenomenon is less pronounced for the fine sand, probably owing to the well-graded nature of the soil sample. The translation of grains is less affected by coordination number than rotation. The results show the effect of grain shape on rotation, as more elongated or plate-like shapes as well as concaved grains tend to exhibit less rotation. This supports the linkage between shape-induced interlocking and rotation of the grains. The rich image-based experimental data from this study will be instrumental for the development and validation of advanced discrete numerical approaches to model the behaviour of shelly carbonate sands.

7. Appendix

The four shape parameters used in this study, I_E, I_F, I_C and I_S were calculated as follows:

$$I_E = \frac{a-b}{a} \tag{5}$$

$$I_F = \frac{b-c}{b} \tag{6}$$

$$I_C = \frac{V_{fill}}{V_{con}} \tag{7}$$

$$I_S = \frac{V_{fill}}{V_s} \tag{8}$$

where V_{fill} is the volume of the grain after being filled, calculated based on the triangular surface mesh described above, V_{con} is the volume of the minimum convex hull that encloses the grain and Vs is the volume of the circumscribed sphere of the grain, with radius R_o (Welzl, 1991). More details can be found in Kong and Fonseca (2018).

Acknowledgement

The authors gratefully acknowledge the financial support provided by the UK Engineering and Physical Sciences Research Council (EPSRC) under the grant MuMShell: Multiscale modelling of shelly carbonate sands for foundation design of offshore structures (EP/N018168/1).

References

Altuhafi, F. N., & Coop, M. R. (2011). Changes to particle characteristics associated with the compression of sands. Géotechnique, 61(6), 459.

Andò, E., Hall, S.A., Viggiani, G., Desrues, J., Bésuelle, P. 2012. Grain-scale experimental investigation of localised deformation in sand: a discrete particle tracking approach. Acta Geotechnica, 7(1), 1–13.

Bar-Kochba, E., Toyjanova, J., Andrews, E., Kim, K.S., Franck, C. 2015. A Fast Iterative Digital Volume Correlation Algorithm for Large Deformations. Experimental Mechanics, 55(1), 261–274.

Bay, B.K., Smith, T.S., Fyhrie, D.P., Saad, M. 1999. Digital volume correlation: three-dimensional strain mapping using x-ray tomography. Experimental Mechanics, 39(3), 217–226.

Bay, B.K. 2008. Methods and applications of digital volume correlation. Journal of Strain Analysis for Engineering Design, 43, 745–760.

Beucher, S., Lantuejoul, C. 1979. Use of watersheds in contour detection. In In Proc. Int. Workshop Image Process, 17-21, Rennes, France.

Bolton, M. D. (2000). The role of micro-mechanics in soil mechanics. CUED/D-Soils/TR313, International Workshop on Soil Crushability Yamaguchi University, Japan

Cil, M. B., Alshibli, K. 2014. 3D Evolution of Sand Fracture Under 1D Compression, Géotechnique, 64(5), 351-364

Coop, M.R. 1990. The mechanics of uncemented carbonate sands. Géotechnique, 40(4), 607–626.

Dijkstra, J., Gaudin, C., White, D. J. 2013. Comparison of failure modes below footings on carbonate and silica sands. International Journal of Physical Modelling in Geotechnics, 13(1), 1-12.

Fonseca, J. 2011. The evolution of morphology and fabric of a sand during shearing. PhD thesis, Imperial College London.

Fonseca, J., O'Sullivan, C., Coop, M., Lee, P. 2013a. Quantifying the evolution soil fabric during shearing using directional parameters. Géotechnique, 63(6), 487–499.

Fonseca, J., O'Sullivan, C., Coop, M., Lee, P. 2013b. Quantifying the evolution of soil fabric during shearing using scalar parameters. Géotechnique, 63(10), 818–829.

Fonseca, J., Reyes-Aldasoro, C.C. Wils, L. 2015. Three-dimensional quantification of the morphology and intragranular void ratio of a shelly carbonate sand. Proc. 6th Int. Symp. Def. Characteristics Geomaterials.

Golightly, C.R. 1989. Engineering properties of carbonate sands. PhD thesis, University of Bradford.

Gonzalez, R.C, and Woods, R.E. 2008. Digital image processing, 3rd edition. Prentice Hall, Inc. Upper Saddle River, NJ, USA.

Hall, S.A., Bornert, M., Desrues, J., Pannier, Y., Lenoir, N., Viggiani, G., Bésuelle, P. 2010. Discrete and continuum analysis of localised deformation in sand using X-ray μCT and volumetric digital image correlation. Géotechnique, 60(5), 315–322.

Henry, M., Pase, L., Ramos-Lopez, C.F., Lieschke, G.J., Stephen, A.R., Reyes-Aldasoro, C.C. 2013. Phagosight: An open-source matlab package for the analysis of fluorescent neutrophil and macrophage migration in a zebrafish model. Plos One, 8(8).

Huang, H.T., Fiedler, H.E., and Wang, J.J. 1993. Limitation and improvement of PIV. Experiments in Fluids, 15(4), 263–273.

Hussein, A.I., Barbone, P.E, Morgan, E.F. 2012. Digital Volume Correlation for Study of the Mechanics of Whole Bones. Procedia IUTAM, 4, 116–125.

Jambunathan, K., Ju, X.Y., Dobbins, D.N., Ashforth-Frost, S. (1995). An improved cross correlation technique for particle image velocimetry. Measurement Science and Technology, 6(5), 507–514

Karatza, Z., Andò, E., Papanicolopulos, S. A., Viggiani, G., Ooi, J. Y. (2019). Effect of particle morphology and contacts on particle breakage in a granular assembly studied using X-ray tomography. Granular Matter, 21(3), 44.

Kikkawa, N., Orense, R.P, Pender, M.J. (2013). Observations on microstructure of pumice particles using computed tomography. Canadian Geotechnical Journal, 50, 1109–1117.

Kong, D., Fonseca, J. (2018). Quantification of the morphology of shelly carbonate sands using 3D images. Géotechnique, 68(3), 249-261

Leclerc, H., PÈriÈ, J.N., Roux, S., Hild, F. 2011. Voxel-scale digital volume correlation. Experimental Mechanics, 51(4), 1–12.

Liu, L., Morgan, E.F. (2007). Accuracy and precision of digital volume correlation in quantifying displacements and strains in trabecular bone. Journal of Biomechanics, 40(15), 3516–3520.

Mahbub, A., Haque, A. 2016. X-ray computed tomography imaging of the microstructure of sand particles subjected to high pressure one-dimensional compression. Materials, 9(11), 890.

Mathworks 2016. Version 9.0 R2016a. The MathWorks Inc., Natick, Massachusetts.

Meidani, M., Chang, C. S., Deng, Y. 2017. On active and inactive voids and a compression model for granular soils. Engineering Geology, 222, 156-167.

Mesri, G., Vardhanabhuti, B. 2008. Compression of granular materials. Canadian Geotechnical Journal, 46, 369–392.

Meyer, F. 1994. Topographic distance and watershed lines. Signal processing, 38(1), 113-125.

Nadimi, S., Fonseca, J. 2018. Image based simulation of one-dimensional compression tests on carbonate sand. Meccanica, 1-10. Open access: https://doi.org/10.1007/s11012-018-0923-2

Randolph, M. F., Jamiolkowski, M. B., Zdravkovic, L. 2004. Load carrying capacity of foundations. In Proc. Skempton Memorial Conf., London, 1, 207-240.

Dijkstra, J., Gaudin, C., White, D. J. 2013. Comparison of failure modes below footings on carbonate and silica sands. International Journal of Physical Modelling in Geotechnics, 13(1), 1-12

Semple, R.M. 1988. The mechanical properties of carbonate soils. In Engineering for calcareous sediments (eds R. J. Jewell and D. C. Andrews), 807–836. Rotterdam, the Netherlands: Balkema.

Shahnazari, H., Rezvani, R. 2013. Effective parameters for the particle breakage of calcareous sands: An experimental study. Engineering Geology, 159, 98-105.

Shi, Y., Yan, W.M. 2015. Segmentation of irregular porous particles of various sizes from X-ray microfocus computer tomography images using a novel adaptive watershed approach. Géotechnique Letters, 5, 299–305.

Smit, R.C.A. 2010. Discrete 3D Digital Image Correlation (DIC) using particle reconnaissance. Master thesis, Delft University of Technology.

Wählby, C., Sintorn, I.M., Erlandsson, F., Borgefors, G., Bengtsson, E. 2004. Combining intensity, edge, and shape information for 2D and 3D segmentation of cell nuclei on tissue sections, Journal of Microscopy, 215(1), 67–76.

Wang, X. Z., Jiao, Y. Y., Wang, R., Hu, M. J., Meng, Q. S., Tan, F. Y. 2011. Engineering characteristics of the calcareous sand in Nansha Islands, South China Sea. Engineering Geology, 120(1-4), 40-47.

Welzl, E. (1991). Smallest enclosing disks (balls and ellipsoids). Lecture Notes in Computer Science 555: 359-370.

Yasufuku, N., Hyde, A. F. L. 1995. Pile end-bearing capacity in crushable sands. Géotechnique 45(4), 663–676.

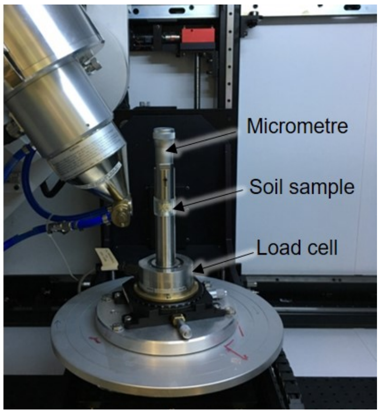

Figure 1: Set-up of the one-dimensional compression tests inside a μCT scanner

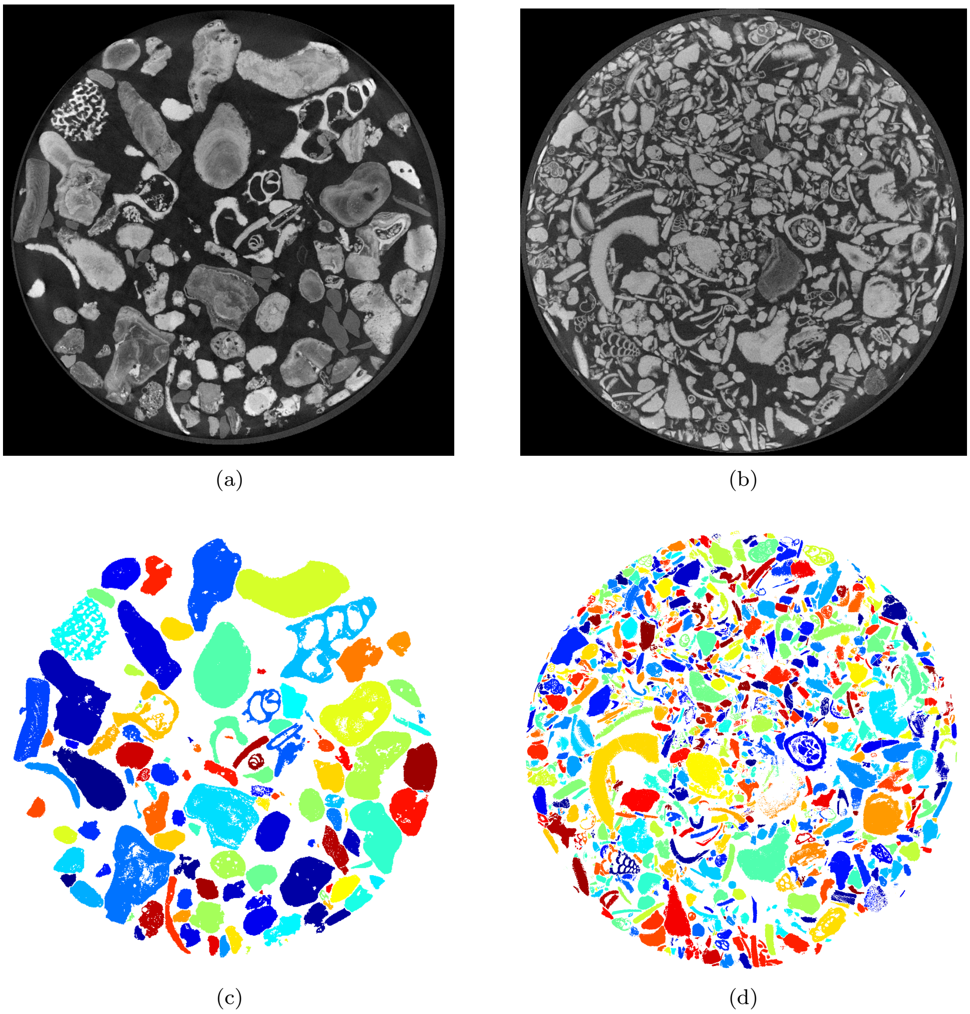

Figure 2: Top view slices through 3D images of the samples prior to loading: (a) CS raw data; (b) FS raw data; (c) CS segmented; (d) FS segmented

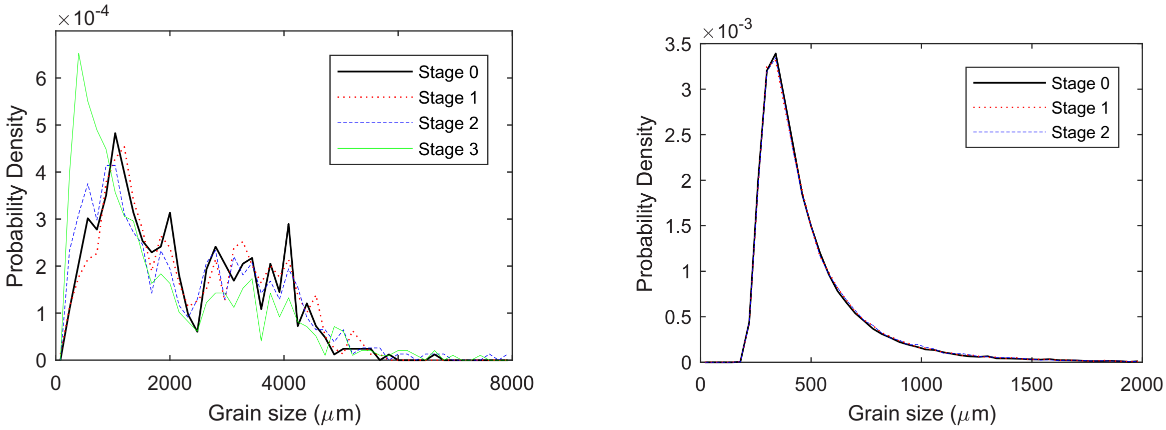

(a) (b)

Figure 3: Evolution of grain size with loading (given by major axis length a): (a) CS; (b) FS

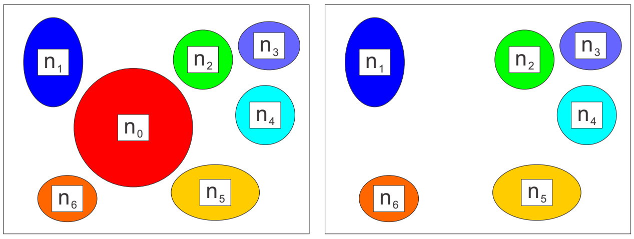

(a) (b)

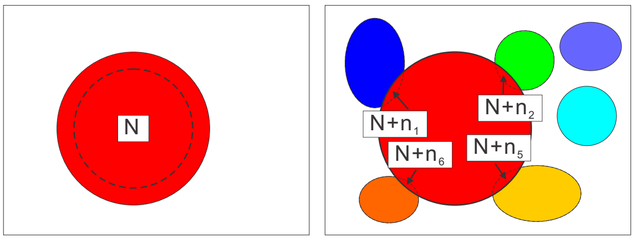

(c) (d)

Figure 4: Illustration of the contact detection algorithm: (a) grain $n-0$ with neighbouring grains; (b) isolated neighbouring grains; (c) dilated and temporarily re-labeled grain $n-0$; (d) identification of in-contact neighbouring grains

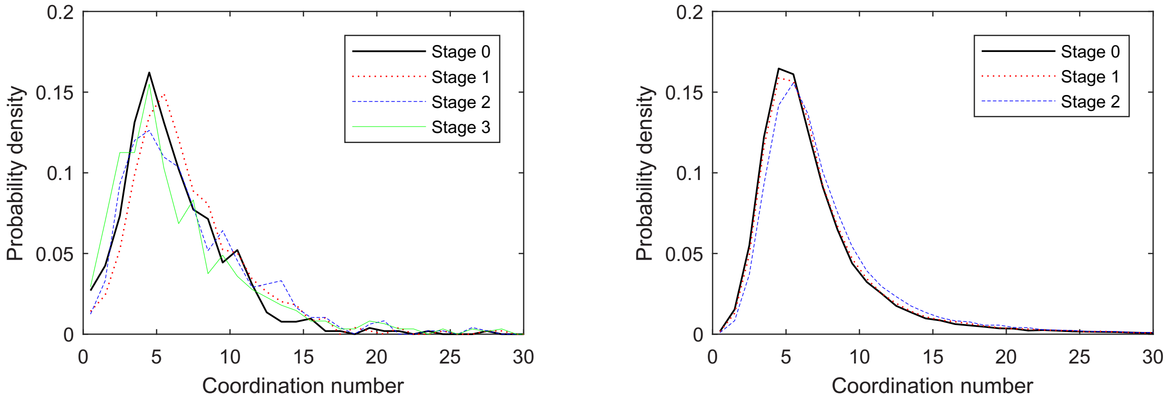

(a) (b)

Figure 5: Evolution of coordination number with loading: (a) CS; (b) FS

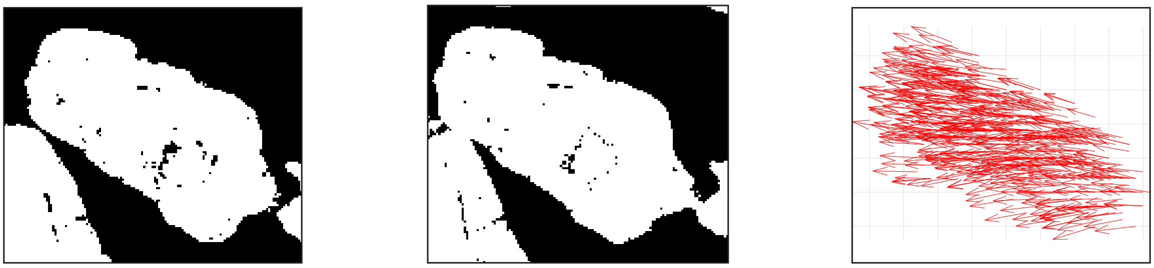

(a) (b) (c)

Figure 6: Illustration of the DVC-reconstruction method: (a) binary grain at reference position; (b) binary grain at target position; (c) associated displacement vectors

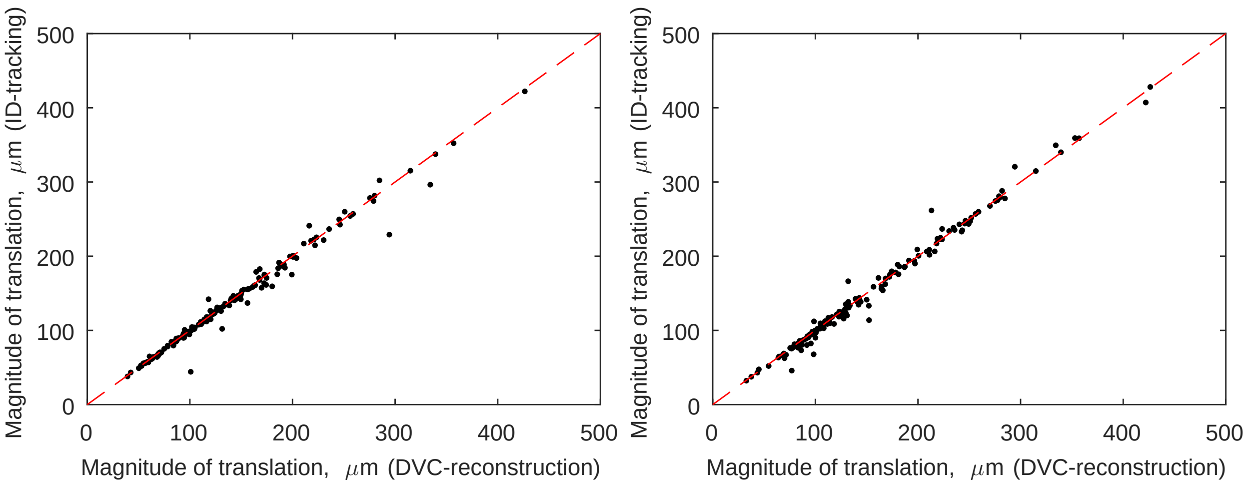

(a) (b)

Figure 7: Comparison of grain translation measured using ID-tracking and DVC-reconstruction methods (showing CS): (a) interval 1-2 (b) interval 2-3

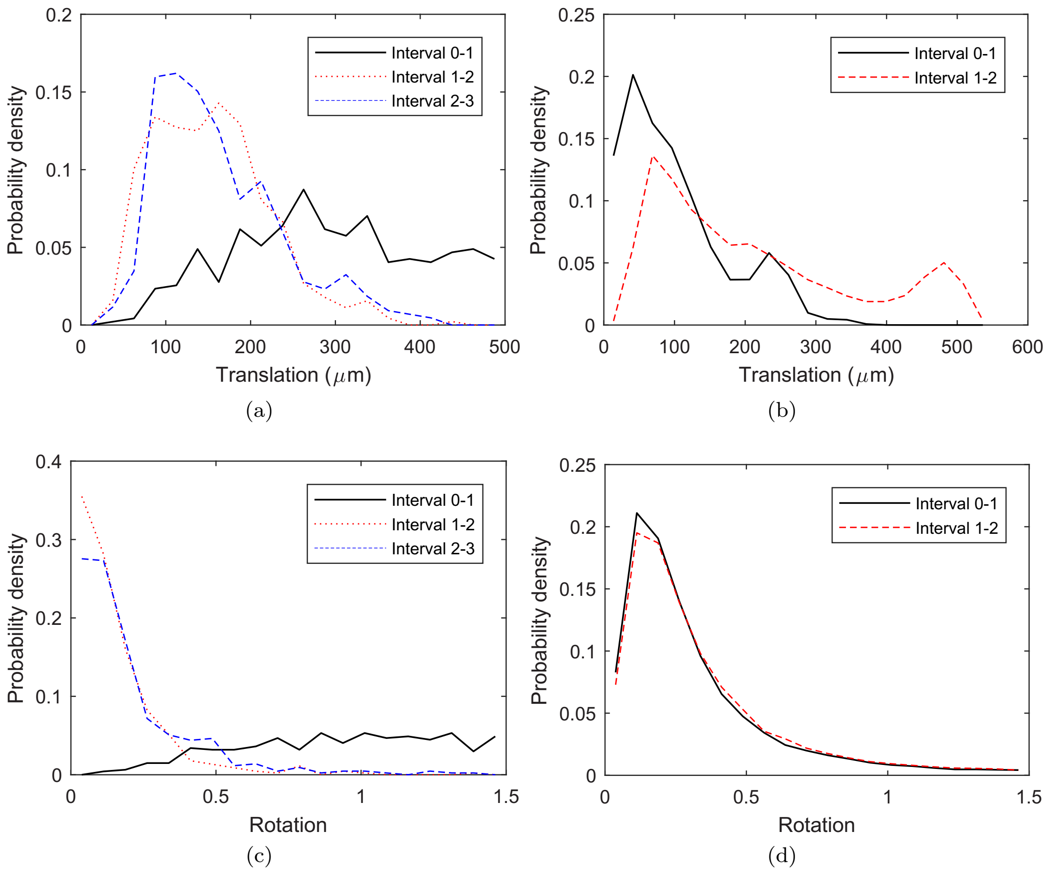

Figure 8: Frequency distribution of grain translation and rotation for different loading intervals: (a) CS translation; (b) FS translation; (c) CS rotation; (d) FS rotation

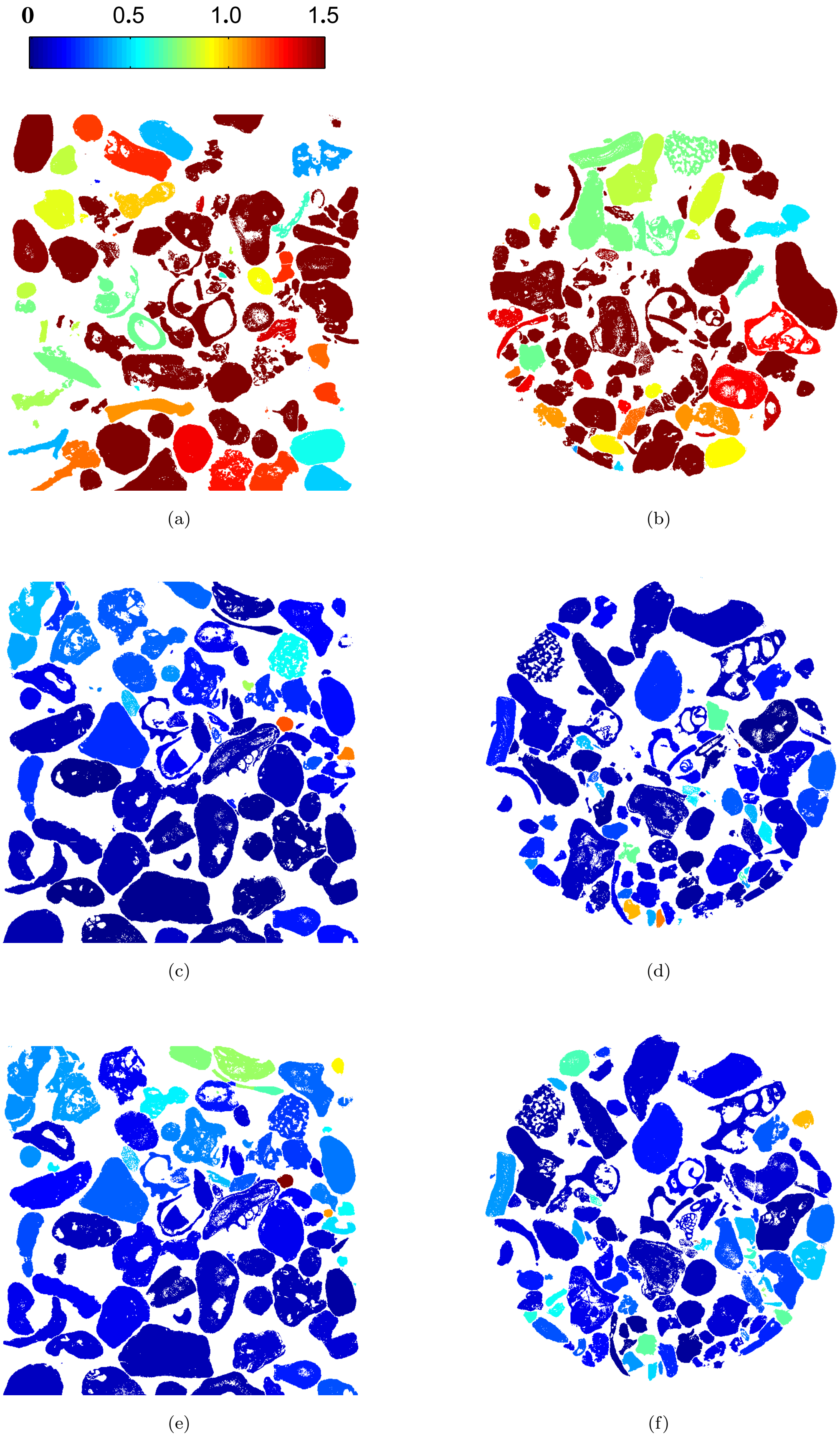

Figure 9: CS sample with each grain coloured by associated rotation factor (showing CS): (a) side view interval 0-1 (b) top view interval 0-1; (c) side view interval 1-2; (d) top view interval 1-2; (e) side view interval 2-3; (d) top view interval 2-3

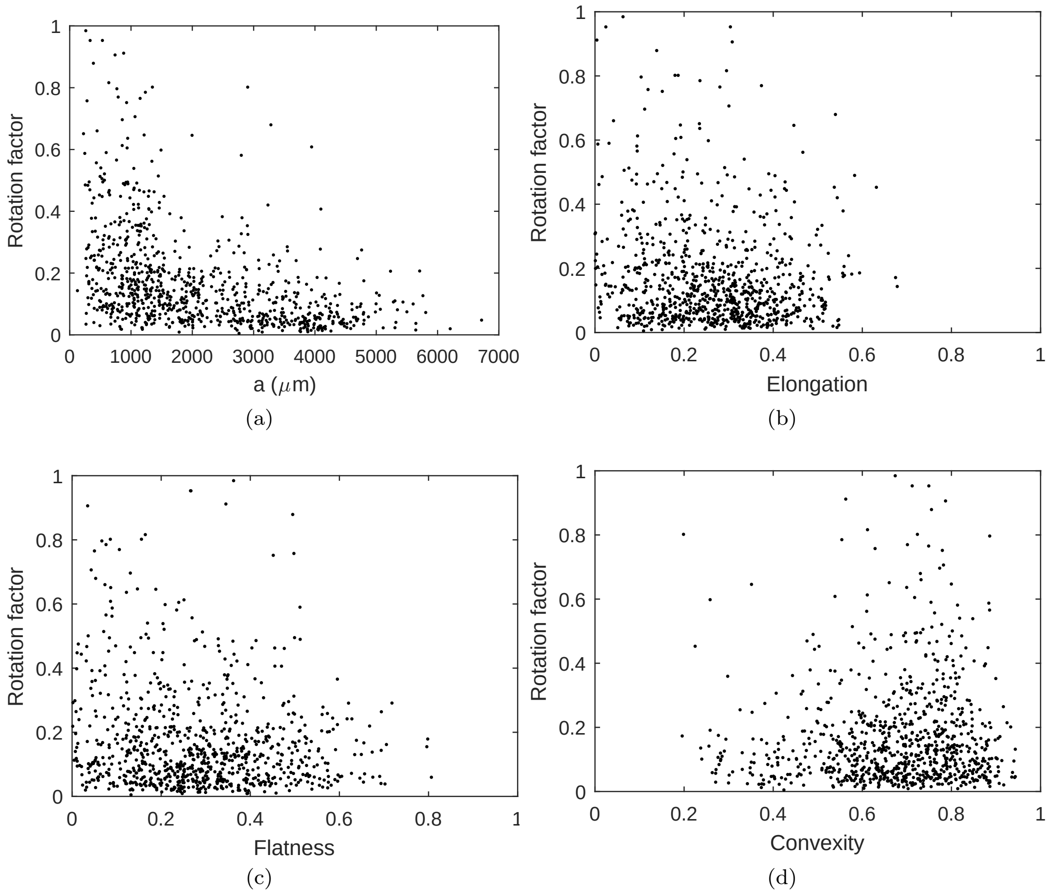

Figure 10: Plot of rotation factor against grain size and shape indices (showing CS): (a) size given by a; (b) elongation; (c) flatness; (d) convexity